

Article

Synthesis of a Multi-Template Molecular Imprinted Bulk Polymer for the Adsorption of Non-Steroidal Inflammatory and Antiretroviral Drugs

Sisonke Sigonya ^{1,*}, Teboho Clement Mokhena ², Paul Micheal Mayer ³, Phumlane Selby Mdluli ²,
Talent Raymond Makhanya ¹ and Thabang Hendrica Mokhothu ¹

¹ Department of Chemistry, Durban University of Technology, Durban 4000, South Africa; talentmakhanya@dut.ac.za (T.R.M.); thabangm1@dut.ac.za (T.H.M.)

² DST/Mintek NIC, Advanced Materials Division, Mintek, 200 Malibongwe Drive, Randburg 2125, South Africa; tebohom@mintek.co.za (T.C.M.); phumlanem@mintek.co.za (P.S.M.)

³ Department of Chemistry and Biomolecular Sciences, University of Ottawa, 10 Marie-Curie Pvt, STEM Complex, Room 342, Ottawa, ON K1N 6N6, Canada; pmmayer@uottawa.ca

* Correspondence: sigonyasonke@gmail.com

Abstract: In this paper, we report the synthesis of a multi-template molecularly imprinted polymer (MIP) to target and extract naproxen, ibuprofen, diclofenac, emtricitabine, tenofovir disoproxil, and efavirenz from wastewater bodies. A bulk polymerization procedure was used to synthesize the MIP and non-imprinted polymer (NIP). The specific recognition sites for each target were obtained through the removal of the imprinted targeted compounds. The interaction of antiretroviral drugs (ARVs) and non-steroidal anti-inflammatory drugs (NSAIDs) compounds with the MIP was studied under various conditions such as pH, mass, concentration, and time factors. The results demonstrated the optimum conditions were 55 mg of MIP, pH 7.0, a concentration of 5 mg L⁻¹, and a contact time of 10 min. For every compound studied, the extraction efficiencies for ARVs and NSAIDs in aqueous solutions was >96%. The adsorption capacity for the MIP was >0.91 mg·g⁻¹. Adsorption obeys a second-order rate, and the Freundlich model explains the adsorption isotherm data. This study demonstrated that the synthesized multi-template MIP has huge potential to be employed for the removal of ARVs and NSAIDs from the environment as well as in drug purification or recovery processes.

Keywords: multi-template molecularly imprinted polymer (MIP); NSAIDs; ARVs; adsorption; second-order isotherm



Citation: Sigonya, S.; Mokhena, T.C.; Mayer, P.M.; Mdluli, P.S.; Makhanya, T.R.; Mokhothu, T.H. Synthesis of a Multi-Template Molecular Imprinted Bulk Polymer for the Adsorption of Non-Steroidal Inflammatory and Antiretroviral Drugs. *Appl. Sci.* **2024**, *14*, 3320. <https://doi.org/10.3390/app14083320>

Academic Editor: Gang Wei

Received: 4 March 2024

Revised: 31 March 2024

Accepted: 11 April 2024

Published: 15 April 2024



Copyright: © 2024 by the authors. Licensee MDPI, Basel, Switzerland. This article is an open access article distributed under the terms and conditions of the Creative Commons Attribution (CC BY) license (<https://creativecommons.org/licenses/by/4.0/>).

1. Introduction

Several studies have revealed that a variety of pharmaceutical substances are regularly discovered in surface waterways, making them a growing environmental and public health concern over the past decade [1–4]. Among these pollutants, antiretroviral (ARV) drugs and non-steroidal anti-inflammatory drugs (NSAIDs) have gained particular attention due to their widespread usage and persistence in aquatic systems. The discharge of these pharmaceutical compounds into natural water bodies, primarily through effluent discharges from sewage treatment plants and hospitals, has raised questions about their potential impacts on aquatic ecosystems and human health [5–8].

ARV drugs, which are essential in the treatment of HIV/AIDS, have dramatically improved the quality of life and life expectancy of individuals living with the disease. However, their presence in water systems poses potential risks, including the development of drug-resistant strains of the virus and adverse effects on aquatic organisms [9,10]. On the other hand, NSAIDs, commonly used to relieve pain and inflammation, can also

be found in aquatic environments due to their extensive use. The environmental consequences of NSAID contamination include disrupted endocrine systems in aquatic organisms and potential risks to human health through the consumption of contaminated water or seafood [11,12]. To address these concerns and mitigate the impact of pharmaceutical pollutants in water systems, researchers have turned to innovative technologies, including molecularly imprinted polymers [13], activated carbon [14], zeolites [15], and silica gel [16], which are conventional choices due to their widespread availability and cost-effectiveness. Activated carbon boasts a high surface area and adsorption capacity, making it suitable for general-purpose adsorption tasks [17]. However, its lack of molecular selectivity and susceptibility to fouling limit its applicability in tasks requiring specific molecular recognition. Similarly, zeolites offer a well-defined pore structure and selective adsorption properties, but their limited scalability and relatively high cost pose challenges for certain applications [18]. Silica gel, known for its good adsorption capacity for polar molecules, is cost-effective and chemically inert but suffers from limited selectivity and susceptibility to hydrolysis [19].

In contrast, molecularly imprinted polymers (MIPs) present a distinct advantage in selective adsorption purposes. MIPs are synthetic materials designed with specific molecular recognition sites that can selectively bind to target compounds, such as pharmaceuticals [20]. Their customizability and high selectivity make MIPs promising candidates for the removal of ARV drugs, NSAIDs, and other pharmaceutical pollutants from water sources [21,22]. By leveraging molecular recognition principles, MIPs offer an environmentally friendly and efficient solution to this emerging environmental challenge. To prepare these MIPs, various important materials are needed, such as a functional monomer and cross-linking agent. A functional monomer is a molecule that is known to be responsible for the binding interactions at imprinted binding sites [20,23]. A functional monomer is utilized in excess compared to moles of a template in a non-covalent imprinting technique to promote the production of template-functional monomer assemblies [24]. The functional monomer in the current study was 2-vinyl pyridine. This monomer can create hydrogen bonding with the carboxylic group of the target molecules and plays a crucial role in the formation of selective binding sites within the MIPs, facilitating the recognition and separation of the target molecule [20]. The functional groups present on the template molecule interact with complementary functional groups within the polymer matrix, in this case, the nitrogen in the pyridine, leading to specific binding and recognition of the target molecule based on chemical compatibility. A cross-linking agent is used to synthesize the polymer to form covalent bonds between polymer chains, creating a network structure that helps to stabilize the polymer structure and create specific binding sites for the template molecule.

Much effort has been directed into utilizing MIPs to extract a single component from a variety of aqueous samples, such as ketoprofen [11,25], and abacavir [12] and tenofovir [26]. However, very few studies have been reported on aqueous solutions employing multi-template MIPs, particularly for the simultaneous removal of ARVs and NSAIDs. Nkosi et al. [14] and Madikizela et al. [17] presented a study on the synthesis, characterization, and optimizations of MIPs for NSAID elimination. They reported on the detection of ibuprofen, naproxen, and diclofenac in aqueous samples employing a multi-template MIP as a selective adsorbent for solid-phase extraction in different investigations and had recoveries above 98% for each target molecule. Progress on the synthesis of templates that can simultaneously remove drugs from different aqueous mediums is essential for their recovery and environmental protection. While these studies have made significant contributions to the field, challenges such as template leakage, polymerization heterogeneity, and scalability limitations still exist. Recent advancements, including the development of novel functional monomers [27,28] and the integration of advanced characterization techniques, offer promising solutions to address these challenges and pave the way for the widespread application of MIPs in pharmaceutical formulations and drug delivery systems.

Therefore, the objective of this paper is to synthesize a multi-template molecularly imprinted polymer that can selectively adsorb non-steroidal inflammatory and antiretroviral

drugs from aqueous medium. The MIPs were prepared using drugs as templates to afford active sites on the surface for targeting specific drugs. The interaction of the templates with the resultant polymer was evaluated using adsorption isotherms, kinetics, and selectivity. The templates' adsorption behavior was carried out under various parameters, such as pH value and concentration. The extraction efficiencies of the MIP and related non-imprinted polymer (NIP) and the formation of a monolayer or multilayer adsorption medium of all templates were assessed. The prepared templates exhibited high adsorption capacities and selectivity for the investigated drugs. The MIP has huge potential to be employed for the removal of these drugs from the environment as well as in drug purification or recovery processes.

2. Experimental

2.1. Chemical Reagents

Diclofenac (DICLO) (98%), Ibuprofen (IBU) ($\geq 98\%$), Naproxen (NAP) ($\geq 98\%$), Emtricitabine (EMI) (98%), Tenofovir disoproxil (TEN0) ($\geq 98\%$), Efavirenz (EFV) ($\geq 98\%$), 2-vinyl pyridine (97%), Ethylene glycol dimethacrylate (98%), 1,1'-azobis-(cyclohexanecarbonitrile) (98%), high-performance liquid chromatography (HPLC) grade acetone ($\geq 99.8\%$), HPLC grade methanol ($\geq 99.8\%$) and toluene (99.7%), liquid chromatography (LC) grade Acetonitrile (99.8%), and 0.1 formic acid in water mixture were all purchased from Sigma-Aldrich, Ltd. (Markham, ON, Canada). Figures 1 and 2 show the structural representation and proposed mechanism of interaction of the functional monomer and the target templates, and Table 1 depicts the physiochemical properties of these templates. The molecular weight, solubility in water, and pKa of target molecules are important factors that can influence the efficiency of separation in MIPs and NIPs. The molecular weight of the target molecule affects the design of the polymer and the selection of functional monomers, while the solubility in water and pKa values can impact the binding affinity and specificity of the polymer. Understanding and considering these parameters can help optimize the formation and performance of MIPs and NIPs for effective separation processes.

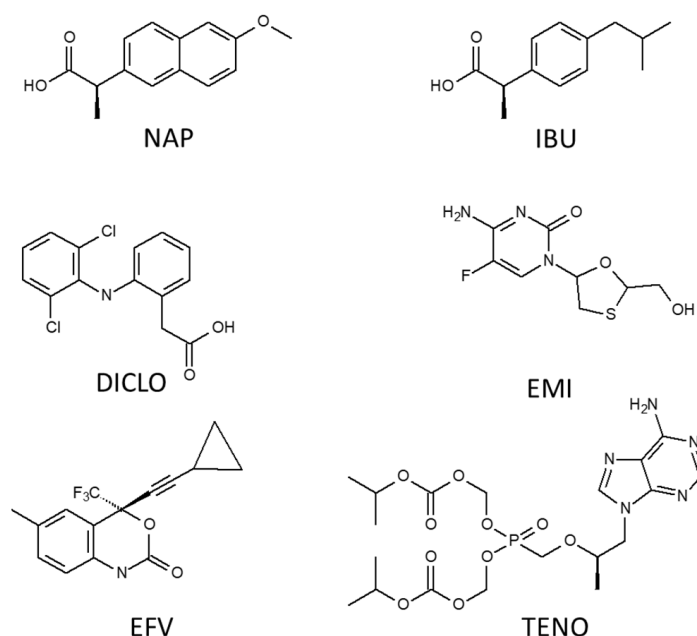


Figure 1. The molecular structures of the respective templates, where NAP = naproxen, IBU = ibuprofen, DICLO = diclofenac, EMI = emtricitabine, EFV = efavirenz, and TENO = tenofovir Disoproxil.

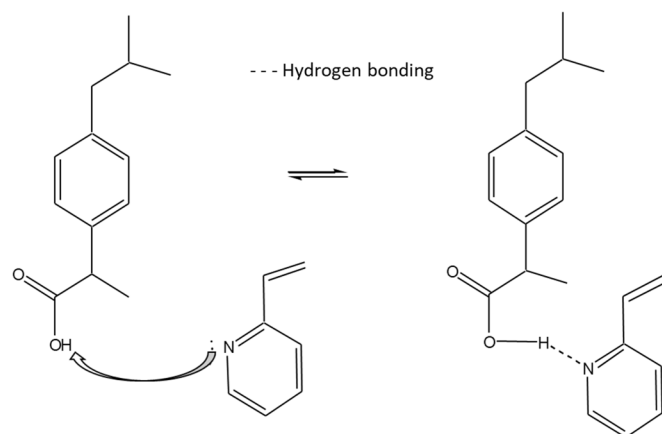


Figure 2. Proposed mechanism of template and functional monomer interaction.

Table 1. Physicochemical properties of target pharmaceuticals [29,30].

Compounds	Formula	Molecular Weight (g/mol)	Water Solubility (mg/L)	pKa
Emtricitabine	C ₈ H ₁₀ FN ₃ O ₃ S	247.25	1.12 × 10 ⁶	2.65
Tenofovir disoproxil	C ₁₉ H ₃₀ N ₅ O ₁₀ P	287.21	13400	3.8
Naproxen	C ₁₄ H ₁₄ O ₃	230.26	15.9	4.2
Diclofenac	C ₁₄ H ₁₁ Cl ₂ NO ₂	296.15	4.52	4.0
Ibuprofen	C ₁₃ H ₁₈ O ₂	206.29	21	4.4
Efavirenz	C ₁₄ H ₉ ClF ₃ NO ₂	315.68	0.093	10.2

2.2. Characterization Techniques

Ultra-high-performance liquid chromatography (UPLC) coupled with UV-VIS detection (LC-UV) and mass spectrometry (LC-MS) were used to perform the chromatographic separation and identification of the NSAIDs and ARVs. LC-UV was performed using an Agilent 1290 Infinity II ultra HPLC System with an Agilent poroshell 120, EC 1.9 μm, 2.1 × 100 mm, C8 reverse-phase column coupled with a binary pump G7120A and multi-sampling system from Agilent Technologies (Waldbronn, Germany). For data collection, the UV-VIS detector was set to 230 and 254 nm for the analysis of the templates and further coupled with an electrospray ionization (ESI) quadrupole time of flight (TOF) mass spectrometer (Waters Synapt G1) for further identification.

Solid state ¹³C CP/MAS NMR was performed on a 4.7T Bruker AVANCE III (Billerica, MA, USA) at 200 MHz. The spectra were collected using a dual channel Bruker 7 mm HX probe with a 4 μs 1H pulse length. At room temperature, the cross-polarization (CP) spectra were recorded with proton decoupling and a recycle delay of 2 s. The ¹³C CP/MAS experiment was conducted on solid glycine and was referred to 176.4 ppm. Cross-polarization contact time was improved to 2.0 ms. Magic-angle-spinning (MAS) was carried out at a rate of 5000 revolutions per second (5 kHz). Infrared spectra of the NIP and MIP were acquired on an Agilent Cary 670 Fourier-Transform infrared (FTIR) spectrometer (Birmingham, AL, USA).

Morphological images of the polymers were obtained with a JEOL JSM-7500F (Tokyo, Japan) field emission scanning electron microscope (SEM). Thermogravimetric analysis (TGA) was performed with a TGA 55 from TA Instruments (San Jose, CA, USA). A platinum pan loaded with ~10 mg was used. The ramp rate was 10 °C per minute from room temperature up to 500 °C for the MIP and NIP. A Brunauer–Emmett–Teller (BET) instrument (Micromeritics Instruments Inc. (Norcross, GA, USA). accelerated surface area and porosimetry System (ASAP) 2020) was used to characterize the surface area, pore size, and pore volume of both polymers. The dry samples were loaded into a glass analysis tube. For activation of the as-synthesized samples, the tube was heated at 120 °C under vacuum for 26 h.

2.3. Synthesis of Polymers

A method by Madikizela and Chimuka [31] was adopted for the synthesis of the molecularly imprinted polymers with minor changes. MIP bulk polymerization was carried out in two phases. In the first stage, 20 mg of 1,10-azobis-(cyclohexanecarbonitrile) was dissolved in 50 mL of toluene, followed by 1.51 mL of ethylene glycol dimethylacrylate. The flask was capped after being purged with nitrogen for 15 min. The reaction was then allowed to proceed for 8 h with steady stirring in an oil bath set at 70 °C. Then, 0.33 mmol of EMI, TENO, NAP, DICLO, IBU, and EFV, respectively, were dissolved in acetonitrile (25 mL), then 0.25 mL 2-vinyl pyridine, 3.85 mL ethylene glycol dimethylacrylate, 60 mg 1,10-azobis-(cyclohexanecarbonitrile), and 25 mL toluene were added. These components were transferred to the reaction product formed in the first stage. The mixture was sealed after being purged with nitrogen for 15 min. For 30 h, the reaction was carried out in an oil bath set at 70 °C. The resulting polymer was oven-dried to a constant mass at 60 °C.

2.4. Template Removal

The imprinted cavities of the templates were voided by performing a Soxhlet extraction process using the dried MIP. A 10% (*v/v*) mixture of acetic acid in methanol in a 250 mL flask was used to wash out the templates from the polymer. This process was repeated multiple times until the UPLC system could no longer detect the templates in the mixture. Furthermore, the polymer was washed with 100% pure acetonitrile to wash off the acetic acid residue. The NIP polymer was treated and washed under the same conditions as the MIP.

2.5. Grinding and Sieving Process of the Polymers

Both the MIP and NIP were milled and sieved into various particles using a 30-mesh hole stainless steel sieve with 595 µm holes. The particles below 595 µm were collected and used subsequently for the extraction experiments. Those above 595 µm were used for characterization.

2.6. Batch Optimizations and Adsorptions Studies

The adsorption studies for both polymers were performed at room temperature using deionized water that had previously been spiked with 5 mg L⁻¹ emtricitabine, tenofovir, naproxen, diclofenac, ibuprofen, and efavirenz. The purpose of this experiment was to investigate the impact of pH (2.5–11), MIP mass (15–55 mg), and adsorption period (10–60 min) on extraction efficiency as well as the effect of concentration range (5–50 mg L⁻¹). During the optimization, a single parameter was altered at a time, while the others remained constant. The mixture was agitated at room temperature for 20 min before being transferred to 3 mL SPE tubes, where the liquid fraction was discarded. Frits were used below and above the polymer to prevent sorbent loss. Experimental extraction efficiency was calculated and carried out in triplicate. Using Equation (1), the extraction efficiency, or the amount of each ARV and NSAID removed by the MIP, was calculated as the difference between the spiking amount (C_0 , mg L⁻¹) and the residual amount in solution after extraction (C_f , mg L⁻¹). The adsorption capacity, or the maximum amount of each ARV and NSAID absorbed by a unit mass of MIP and NIP, was calculated using Equation (2), where V is the volume (L) of the solution, and W represents the mass of the polymer in (g) [32–34].

$$\text{Extraction efficiency (\%)} = \frac{(C_0 - C_f)}{C_0} \times 100 \quad (1)$$

$$\text{Adsorption capacity (mg} \cdot \text{g}^{-1}\text{)} = \frac{(C_0 - C_f)}{W} V \quad (2)$$

For pseudo-first-order and pseudo-second-order kinetic models, Equations (3) and (4) were used to illustrate the adsorption method. The adsorption mechanism was described

using the model with the highest R^2 value, where Q_e and Q_t are the adsorption capacity parameters ($\text{mg}\cdot\text{g}^{-1}$) at equilibrium and at time t (min), respectively. K_1 and K_2 are the Lagergren pseudo-first-order and pseudo-second-order rate (min^{-1}) sorption constants [30,35].

$$\text{Log}(Q_e - Q_t) = \text{Log}Q_e - \frac{K_1 t}{2.303} \quad (3)$$

$$\frac{t}{Q_e} = \frac{1}{K_2 Q_2} + \frac{t}{Q_e} \quad (4)$$

The linearized forms of the Freundlich and Langmuir isotherms were used to describe the extent of adsorption and the isothermal analysis of the polymers, respectively, where n denotes adsorption intensity or surface heterogeneity, C_e the target molecules adsorption capacity ($\text{mg}\cdot\text{g}^{-1}$), K_f is the Freundlich constant, q_e is the compound uptake in at equilibrium in ($\text{mg}\cdot\text{g}^{-1}$), and Q_{max} the maximum adsorption capacity ($\text{mg}\cdot\text{g}^{-1}$), and K_L the Langmuir adsorption equilibrium constant. The intercepts and slopes of the linear plots of C_e/Q vs. C_e were used to calculate the constants K_L and Q_{max} (Equations (5) and (6)).

$$\text{Log}q_e = \text{Log}K_f + \frac{1}{n}\text{Log}C_e \quad (5)$$

$$\frac{C_e}{Q} = \frac{C_e}{Q_{max}} + \frac{1}{Q_{max} \times K_L} \quad (6)$$

2.6.1. Selectivity Experiments

The selectivity of the MIP for ARVs and NSAIDs was determined in batch rebinding experiments at room temperature using optimum conditions, which were deionized water (pH 7.0) previously spiked with 5 mg L^{-1} mixtures of EMI, TENO, NAP, DICLO, IBU, and EFV, and acetaminophen (competitor). The spiked solution (10 mL) was put into a flask with 55 mg of MIP. The resultant solution was agitated for 15 min (360 rpm) at room temperature before being placed into a 3 mL SPE tube. Two polypropylene frits with pore sizes of $10 \mu\text{m}$ were placed below and above the MIP to prevent sorbent loss, and the liquid portions were discarded. Following that, the concentration of unadsorbed compounds in the solution was assessed using LC-MS. The ARVs and NSAIDs were then competitively absorbed from the mixture in the presence of acetaminophen. Using Equation (7), the effect of imprinting on selectivity was estimated, where K_d (mg g^{-1}) is the distribution coefficient, C_0 is the initial solution concentration (mg L^{-1}), C is the final solution concentration (mg L^{-1}), V (L) is the solution volume, and W (g) is the polymer weight. Furthermore, in the presence of a competitor, the selectivity coefficient for the binding of ARV and NSAID compounds was estimated using Equation (8), where K is the selectivity coefficient. In addition, the MIPs selectivity coefficient (K') was calculated as described in Equation (9).

$$K_d = \frac{C_0 - C}{W} V \quad (7)$$

$$K = \frac{K_d(\text{Target})}{K_d(\text{Competitor})} \quad (8)$$

$$K' = \frac{K_{\text{MIP}}}{K_{\text{NIP}}} \quad (9)$$

2.6.2. Swelling Experiments

An empty 50 mL centrifuge tube was filled with 55 mg of the polymer and 10 mL of water. At room temperature, swelling was allowed to occur at different time intervals ranging from 10 to 60 min. The tube's contents were then centrifuged at 4000 rpm. Excess solvent was discarded, and the wet polymer mass was measured. Equation (10) was used

to compute the swelling capacity. Where M_w is the mass of the wet polymer, M_d is the mass of the dry polymer.

$$\text{Swelling capacity} = \frac{M_w - M_d}{M_d} \times 100 \quad (10)$$

3. Results and Discussion

3.1. Surface Chemistry

The solid-state ^{13}C CP/MAS NMR spectra for the MIP and NIP are shown in Figure 3. The baseline was adjusted, and the relevant peaks were identified between 0 and 200 ppm spectral regions. There seemed to be no dissimilarities between the chemical shifts and signal intensities of the polymers. This suggested that the polymer materials are chemically the same. Resonances were observed corresponding to the various methyl groups represented by the wide peak at 23 ppm. Other methylene groups were found to correspond to the cross-linker agent used at 47 and 65 ppm, as well as the carbonyl CO_2R group observed at 175 ppm. Given the kind of polymer synthesis and mechanism of imprinting, which involves a considerable quantity of EGDMA and 2-VP, these results were anticipated. All signals could be assigned in accordance with the estimated polymer design, and the appropriate peaks matched the results from previous studies [30–32]. Nkosi et al. [13] reported the same chemical shifts as those used in the process for the analysis of MIP and NIP of NSAIDs and used the same functional monomer. At the same time, carbonyl clustering in CO_2R is clearly visible at the far end, which is consistent with what is found in the literature [30,32].

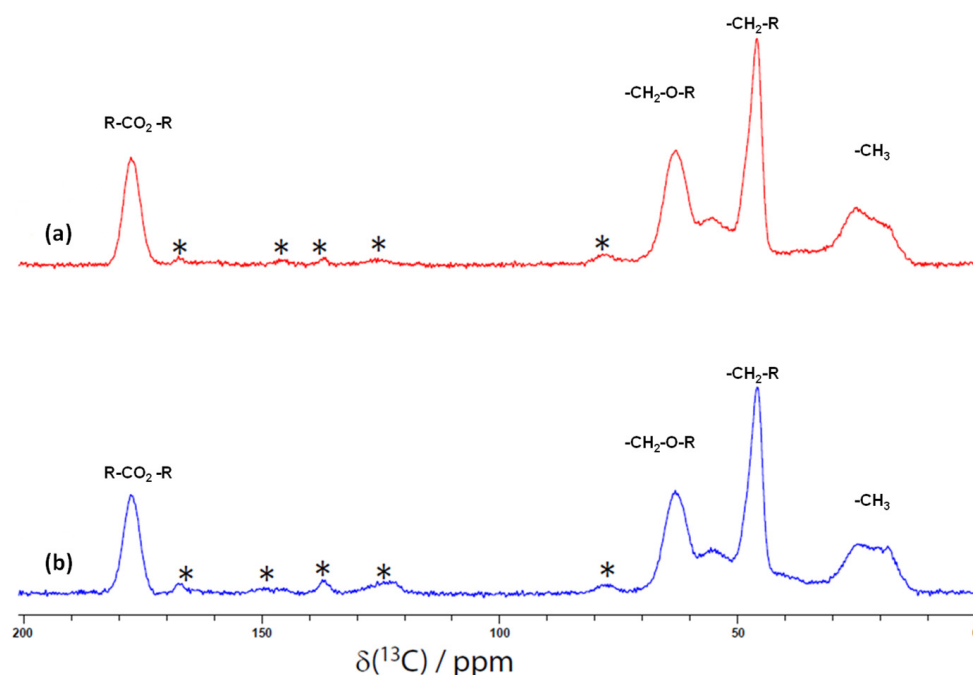


Figure 3. Solid-state ^{13}C CP/MAS NMR spectra for (a) the MIP and (b) the NIP. * Denotes solvent peaks.

Figure 4 shows FTIR spectra of the synthesized and washed MIP and NIP. It can be observed that the IR spectra of the polymers are very similar in terms of bands, positions, and shape, which is consistent with the fact that both polymers were created using the same monomer, cross-linker, and initiator. The interface between templates and monomer provided variable peaks in the spectra, with MIPs exhibiting a wide OH stretching vibration peak at 3500 cm^{-1} , the OH formed a bond that overlaps with that from the NH from the MIP, and this peak slightly smooths out in the NIP. These peaks are associated with the carboxylic group (COOH) of methacrylic acid. Because of the methylene group in 2-VP and

EGDMA, the -CH_2 stretching peak was also seen at 2900 cm^{-1} . At 1700 cm^{-1} , the carbonyl group C=O stretching peak was seen in both MIP and NIP, which might have arisen from the template and cross-linking molecules. Weak bands from 1600 cm^{-1} to 1200 cm^{-1} , as well as the sharp band at 1100 cm^{-1} in the MIP spectrum, indicate the existence of an aromatic ring from the 2-VP. All the notable peaks matched the data from previous studies [30], where they reported the same stretchings and the presence of these functional groups around the same wavelength.

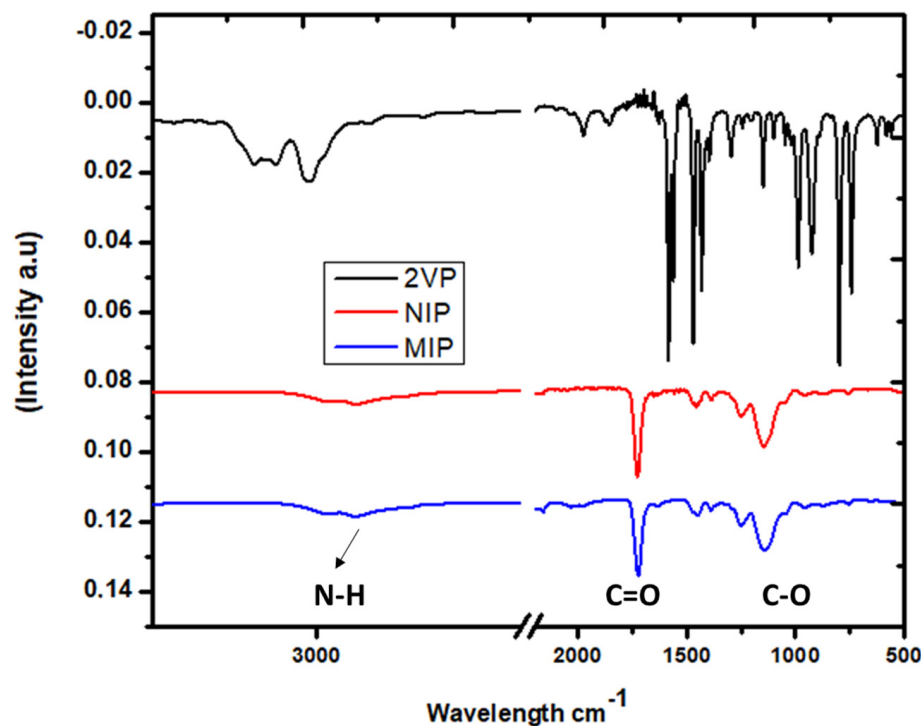


Figure 4. FTIR spectrum of the MIP, NIP, and the functional monomer 2-vinylpyridine (2-VP).

3.2. Morphology Analysis

3.2.1. SEM

The surface morphology and particle size of both the MIP and NIP were examined using SEM, as shown in Figure 5. The surface of the control polymer (NIP) was found to be smoother than that of the MIP, as it did not have the target template to form the desired cavities. Smaller pores are observed in the NIP images due to the polymerization process, which can create minor defects that are non-binding specific to create this porosity. Other factors, such as the solvent and cross-linking effect density, can contribute to the porosity of the NIP, as when these solvents are being evaporated, they might leave a void. The MIP, on the other hand, had a rough surface once the templates were removed. These rough surfaces can be attributed to the formation of cavities during the synthesis process and washing out of the template process; when these templates are removed, they form their desired specific binding pores (cavities) [36,37]. A prior study found that the roughness of MIP particles might result in a higher surface area than the control polymer [38]. As a result, the MIP outperforms the control polymer in adsorbing analytes of interest.

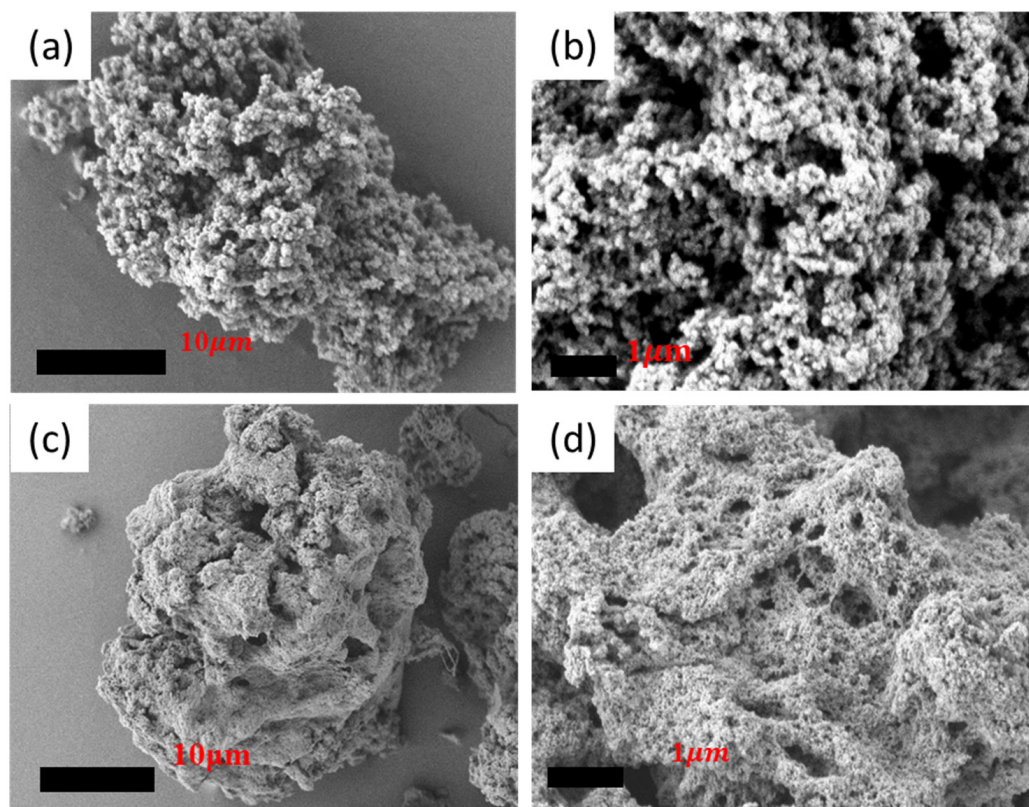


Figure 5. SEM surface morphologies: (a) NIP SEM image, with an expanded view in (c) MIP SEM with an expanded view in (b,d).

3.2.2. Brunauer, Emmett, and Teller (BET) Analysis

BET was used to study the surface area, surface volume, and porosity of the MIP and NIP, as tabulated in Table 2. The surface area of polymers has a considerable impact on compound adsorption. According to the BET data shown in Table 2, the MIP had a higher surface area, pore volume ($425 \text{ m}^2\text{g}^{-1}$), and total area in the pore ($258 \text{ m}^2\text{g}^{-1}$) than the NIP with 347 and $201 \text{ m}^2\text{g}^{-1}$ of surface area and total area in the pore, respectively. This is consistent with the desired imprinting. With the NIP, these areas are smaller because there were no target templates for specific binding; however, smaller cavities or voids are formed, possibly by solvent evaporation or cross-linking density, as mentioned earlier. The same pattern has been observed in a previous study of NSAID adsorption on similar polymers by Madikizela et al. [39]. It was reported that the synthesized MIP and NIP surface area were 282 and $232 \text{ m}^2\text{g}^{-1}$, respectively. Qwane et al. [32] reported surface area results with the ARV drug abacavir imprinted MIP and its NIP analog of $372 \text{ m}^2\text{g}^{-1}$ for both polymer materials. However, the surface area and total pore volume values are significantly larger in this study. This might be because more target compounds are used in this study that are of different classes; therefore, a larger surface area is required to accommodate the six-target compared to the three-target and single-target they were investigating in their studies. Polymers with larger surface areas are more effective in adsorbing water pollutants. There are more binding sites that are scattered in the cavity, suggesting that there is a greater imprinting impact for the MIP compared to the NIP. Also, looking at the total pore areas of the polymers, the MIP has a larger pore size area suggesting that there are more cavity imprints in the MIP as opposed to the NIP.

Table 2. BET polymer analysis.

Polymer	Surface Area (m^2g^{-1})	Total Pore Volume (cm^3/g)	Average Pore Diameter (\AA)	Total Area in Pores (m^2g^{-1})	Average Particle Size (nm)
MIP	425	0.345	44.2	258	14.1
NIP	347	0.393	45.3	201	17.3

3.2.3. Thermal Properties

Figure 6 shows the TGA curves of synthesized MIP and NIP. The TGA was performed to study the thermal stability, uniformity, and binding affinity effects of the polymer materials in case that they are subjected to high temperatures. The analysis was run over a 0–500 °C temperature range. Two disintegration peaks are observed at slightly different temperatures for both the MIP and NIP, suggesting the collapse of the material at both points. The initial backbone decomposition of both these polymers is observed at 275 °C and 278 °C, respectively, as seen in Figure 6a,b, the backbone of both the washed MIP and NIP disintegrated, resulting in a considerable weight loss of nearly 90%. A similar polymer backbone collapse was observed at comparable temperatures of 280 °C in a study by Nkosi et al. [13] when they synthesized the polymers under the same circumstances utilizing the bulk polymerization process. The difference between the curves produced for washed NIP and washed MIP is that the MIP has a second decomposition peak between 371 and 444 °C that is below 15 mass % (compared to the same peak in the NIP that is over 30%). The discrepancy might be due to structural differences imposed during the template removal process of the MIP; there might be residual template molecules or template-related impurities in the MIP. These remaining molecules may interact with the polymer, affecting its thermal stability and resulting in the observed disintegration phases. During the imprinting process, the binding of template molecules to functional monomers may result in chemical bonds or interactions that affect the thermal stability of the polymer. These interactions might be missing from the NIP. It is possible that the molecular imprinting process introduces structural heterogeneity within the MIP, leading to varying decomposition behaviors for different portions of the polymer. Thermal breakdown for both polymers is observed at 445 °C. These findings are consistent with those found in the literature [11,13]. As a result, the thermal stability of these polymers was regarded as adequate because their applications were made at ambient temperature, which revealed slight irregularities in both materials but showed uniformity in the synthesis process of these materials.

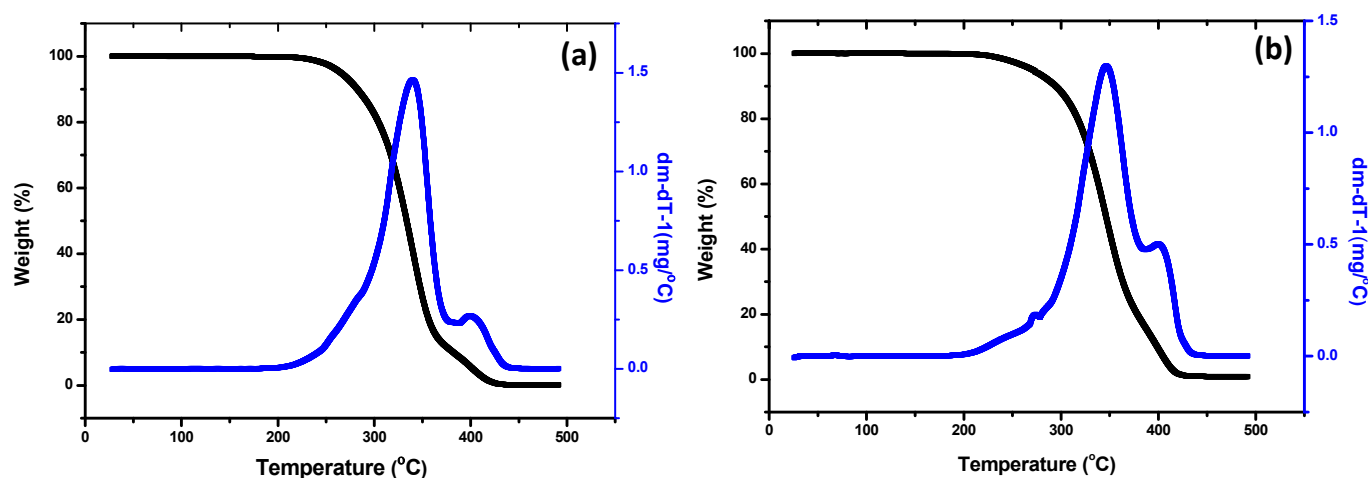


Figure 6. Thermal decomposition of (a) MIP and (b) NIP by TGA.

3.3. Adsorption Studies

3.3.1. Effects of pH

The pH of the water solutions was adjusted to facilitate the monomer–template interaction. The pH was measured in the 2.5–10 range (Figure 7). Various recoveries were observed for the target molecules, especially for emtricitabine, tenofovir disoproxil, and naproxen. EMI has very stable recoveries throughout the various pH mediums, with recoveries above 100%, which was different from TENO, which had low recoveries of 49, 49, 76, and 19% across the pH range. Both of these drugs are nucleoside reverse transcriptase inhibitors and, at a pH of 4, should be more in their neutral or protonated state, which makes the adsorption of the material more effective. However, higher recoveries were seen for its more negative state at more neutral conditions at pH 7 (76%). An electrostatic repulsion was expected in a neutral state due to the type of polymer adsorption material designed; this was not observed. A slight decrease in recoveries was observed for other compounds like NAP, which ranged above 100% under acidic conditions to 71% under neutral conditions. In a previous study [30], it was found that above a pH of 4, the maximum adsorption efficiency decreased due to hydroxide ion interferences in the MIP cavities. Overall, a pH of 7 was opted for in this study as it gave the best overall performance for the six targets.

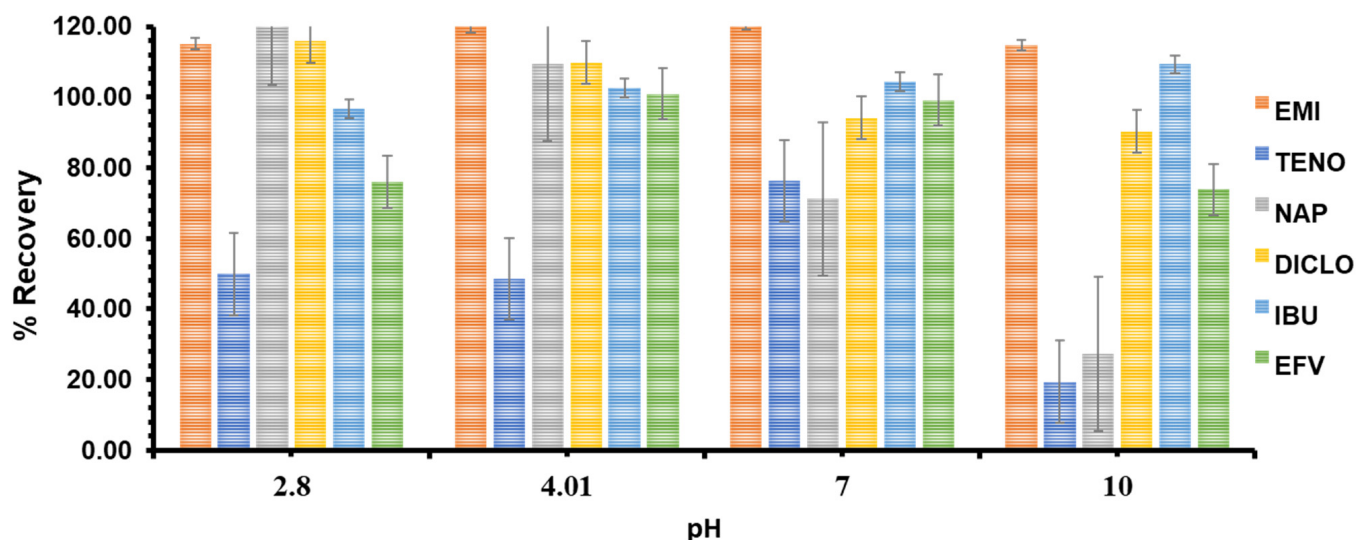


Figure 7. pH effects on the adsorption of ARVs and NSAIDs.

3.3.2. Effects of Polymer Mass

Batch adsorption of the MIP was conducted with polymer masses ranging from 15 to 55 mg, respectively, to find the optimum adsorption mass that will be used throughout the experiments whilst other parameters such as sample pH (7.0), target component concentration ($5 \text{ mg} \cdot \text{L}^{-1}$), and sample volume (10 mL) remained fixed. High recoveries were observed across all masses, with extraction efficiencies ranging from $>83\%$. A mass of 55 mg, as shown in Figure S1, had the best results for all target compounds, as expected from its greater mass and, thus, greater surface area. The MIP (Figure S1a) exhibited superior extraction efficiencies when compared to the NIP (Figure S1b).

3.3.3. Effects of Initial Concentration

As illustrated in Figure S2a,b, the adsorption capacity derived using Equation (2) is plotted as a function of the initial target molecule concentration in the range of 5 to $50 \text{ mg} \cdot \text{L}^{-1}$. The results show a linear relationship between the two for the MIP. In the case of NIP, there is an increase in adsorption with an increase in target molecule concentration. However, a decrease in adsorption efficiency was observed for NAP and IBU as their concentrations reached $40 \text{ mg} \cdot \text{L}^{-1}$. This decrease was not observed for the MIP because it has the designed imprints of the template molecules. Similar trends were observed

in other multi-template studies for MIP adsorption [12]. High adsorption capacities of EMI and TENO, the two ARV drugs, were observed in the NIP with capacities of 49.05 and 22.85 mg·g⁻¹, respectively. This might be due to the flexibility of the non-imprinted polymer to fit the size of these compounds with no steric hindrance. Also, as seen in the SEM and BET results above, the NIP has non-distinct cavities with a larger total pore volume than the MIP; hence, these two compounds with larger molecular weight have been adsorbed more in this material (Figure 5).

3.3.4. Effects of Contact Time

The study investigated how contact time influences extraction efficiency. This was performed by observing the efficiency over various time periods, maintaining constant conditions: a pH of 7.0, an initial concentration of 5 mg L⁻¹, an adsorbent weight of 55 mg, and a total sample volume of 10 mL. Extraction efficiencies greater than 96% were achieved within 10 min of interaction time (Figure S3). In the following experiments, a contact duration of 10 min was used to ensure the regularity of target drug absorption from aqueous samples. Similar observations were reported in the literature [17].

3.4. Adsorption Kinetics

3.4.1. Adsorption Isotherms

Adsorption isotherms may be used to describe how much material is adsorbed as a function of initial concentration at constant temperature, which in this case was ambient temperature. The linear versions of the Langmuir and Freundlich isotherms were used to assess the adsorption data (Table 3). Based on the observed R², the Freundlich isotherm appears to be the best descriptor of the adsorption isotherm. The Freundlich isotherm, characterized by its non-linear nature, suggests a heterogeneity in the binding sites' adsorption capacity of the polymer. The preference for the Freundlich isotherm over the Langmuir indicates that the adsorption process for both MIP and NIP surfaces is not limited to a single monolayer. Instead, it suggests the formation of multilayers of adsorbate molecules on the polymer surface. Moreover, the affinity of both these polymer materials implies potential application, including but not limited to separation purification processes. The values of 1/n for each drug provide insights into the surface characteristics, adsorption intensity, and non-linearity in the adsorption process. These values help us understand the adsorption behavior of each drug and its interaction with the adsorbent surface. Two groups of drug compounds can be discerned based on similarities in their 1/n values. Emtricitabine (1.1968) and ibuprofen (16.359) both exhibit heterogeneous surfaces, suggesting diverse adsorption sites. However, emtricitabine demonstrates a moderate adsorption intensity, implying a balanced adsorption process across different concentrations. Conversely, the drug ibuprofen displays a low adsorption intensity, indicating less favorable adsorption conditions. Moreover, while emtricitabine shows moderate non-linearity in adsorption, ibuprofen demonstrates high non-linearity, indicating a steep increase in adsorption capacity with decreasing concentration.

Similarly, tenofovir (0.302) and diclofenac (0.7003) present highly heterogeneous surfaces conducive to strong adsorption at low concentrations. Despite this similarity, both drugs exhibit a moderate adsorption intensity, suggesting favorable adsorption conditions. Moreover, their non-linearity in adsorption is high, with a steep rise in adsorption capacity observed as concentration decreases.

Individually, naproxen (2.487) showcases considerable surface heterogeneity, potentially with varying adsorption sites. Its relatively high adsorption intensity suggests weaker adsorption at low concentrations, while moderate non-linearity in adsorption implies a moderate increase in adsorption capacity with decreasing concentration. In contrast, efavirenz (1.5028) demonstrates a relatively homogeneous surface with consistent adsorption sites. The moderate adsorption intensity observed suggests a balanced adsorption process, while moderate non-linearity in adsorption indicates a gradual increase in adsorption capacity with decreasing concentration. The K_f values indicate the adsorption

behavior of the adsorbent material. For $K_f = 0.6943$ and $K_f = 0.8050$, moderate adsorption capacities are observed, suitable for efficient adsorption processes in wastewater treatment or purification applications. Conversely, for $K_f = 5.3002$ and $K_f = 4.3672$, significantly higher adsorption capacities are evident, which is ideal for the thorough removal of solutes or pollutants from solutions, such as in environmental remediation or industrial processes. Lastly, for $K_f = 0.0389$ and $K_f = 0.0535$, low adsorption capacities are observed, which may find utility in applications requiring selective adsorption or trace contaminant removal.

Table 3. Adsorption Isotherms.

Polymer	Langmuir Isotherm (Equation (6))			Freundlich Isotherm (Equation (5))		
	Compound	R^2	Intercept	1/n	K_f	R^2
MIP	Emtricitabine	0.6124	−0.1977	1.1968	0.6943	0.9869
	Tenofovir disoproxil	0.9709	−0.7240	0.302	5.3002	0.9150
	Naproxen	0.6227	−0.0942	2.487	0.8050	0.8139
	Diclofenac	0.8222	0.6402	0.7003	4.3672	0.9311
	Ibuprofen	0.9840	−1.4099	16.359	0.0389	0.7001
	Efavirenz	0.8525	−1.2718	1.5028	0.0535	0.9313
	NIP	Emtricitabine	0.8854	1.1022	0.5594	15.929
Tenofovir disoproxil		0.7598	1.0834	0.7247	12.117	0.7425
Naproxen		0.9856	0.277	0.4303	1.8958	0.9683
Diclofenac		0.9592	0.6221	0.6456	4.1889	0.9840
Ibuprofen		0.9585	0.0919	0.4199	1.2356	0.6853
Efavirenz		0.8784	0.8577	0.7603	7.2061	0.9812

3.4.2. Kinetic Modelling

The rate of ARV and NSAID adsorption by MIP and NIP was measured as a function of time. If second-order kinetics is used, the plot of t/Q vs. t should provide a straight line. The values K_2 and Q_e were computed from the intercept and slope of the linear plots of C_e/Q vs. C_e , respectively; the data is shown in Table 4. The kinetic modeling results showed that the adsorption process followed pseudo-second-order kinetics as they better obeyed a straight line. The adsorption capacities (Q_e) were 0.90, 0.83, 0.06, 0.83, 0.07, and 0.13 $\text{mg}\cdot\text{g}^{-1}$ for EMI, TENO, NAP, DICLO, IBU, and EFV, respectively. These adsorption capacities were lower in the MIP than in the NIP. For instance, tenofovir disoproxil has an adsorption capacity of 3.58 $\text{mg}\cdot\text{g}^{-1}$ in the NIP compared to 0.83 $\text{mg}\cdot\text{g}^{-1}$ in the MIP. This could be due to the flexibility of the NIP, which has a smoother surface and larger pore size diameter than the MIP, as mentioned earlier in the paper. The pseudo-second-order kinetic model results fit well with the Freundlich isotherm.

Table 4. Calculated results of Kinetic Models.

Polymer	Compounds	Pseudo-First-Order	Pseudo-Second-Order		
		R^2	R^2	K_2 ($\text{mg}\cdot\text{g}^{-1}\text{min}^{-1}$)	Q_e ($\text{mg}\cdot\text{g}^{-1}$)
MIP	Emtricitabine	0.86	1.00	2.75	0.90
	Tenofovir disoproxil	0.61	1.00	3.47	0.83
	Naproxen	0.50	0.90	3.19	0.06
	Diclofenac	0.88	1.00	1.16	0.83
	Ibuprofen	0.86	0.83	0.07	0.07
	Efavirenz	0.86	1.00	2.07	0.13

Table 4. Cont.

Polymer	Compounds	Pseudo-First-Order		Pseudo-Second-Order	
		R^2	R^2	K_2 ($\text{mg}\cdot\text{g}^{-1}\cdot\text{min}^{-1}$)	Q_e ($\text{mg}\cdot\text{g}^{-1}$)
NIP	Emtricitabine	0.84	0.98	0.56	0.92
	Tenofovir disoproxil	0.90	1.00	0.73	3.58
	Naproxen	0.75	0.99	0.43	2.91
	Diclofenac	0.63	1.00	0.65	3.75
	Ibuprofen	0.92	0.92	0.42	0.10
	Efavirenz	0.84	0.92	0.76	0.92

3.5. Swelling Behaviour

Over a one-hour period, the swelling capacity (W) of the polymers was studied using the swelling experimental data explained earlier in Section 2.6.2. Figure 8 depicts the polymers inflating rapidly after 10 min, then decreasing as they approached equilibrium and reaching a plateau between 50 and 60 min. The polymers reached equilibrium at 0.48 and 1.25 $\text{g}\cdot\text{g}^{-1}$ NIP and MIP, respectively. The swelling might be caused by the N-group of 2-vinyl pyridine, which was employed in the polymerization. These findings suggest that water penetrates the polymer network, reducing the osmotic pressure differential between the solution and the polymer and thereby slowing water diffusion [33]. Furthermore, the swelling of the MIP allows water to infiltrate into cavities, increasing interaction with the target chemicals. The MIP's higher swelling capacity also implies the MIP is more prone to swelling in water than the NIP due to the specific imprints and the chemical nature of the imprints within the MIP, which allows greater interaction with the solvent. This is one of the desired outcomes of molecular imprinting since it gives the polymer selectivity and recognition capabilities.

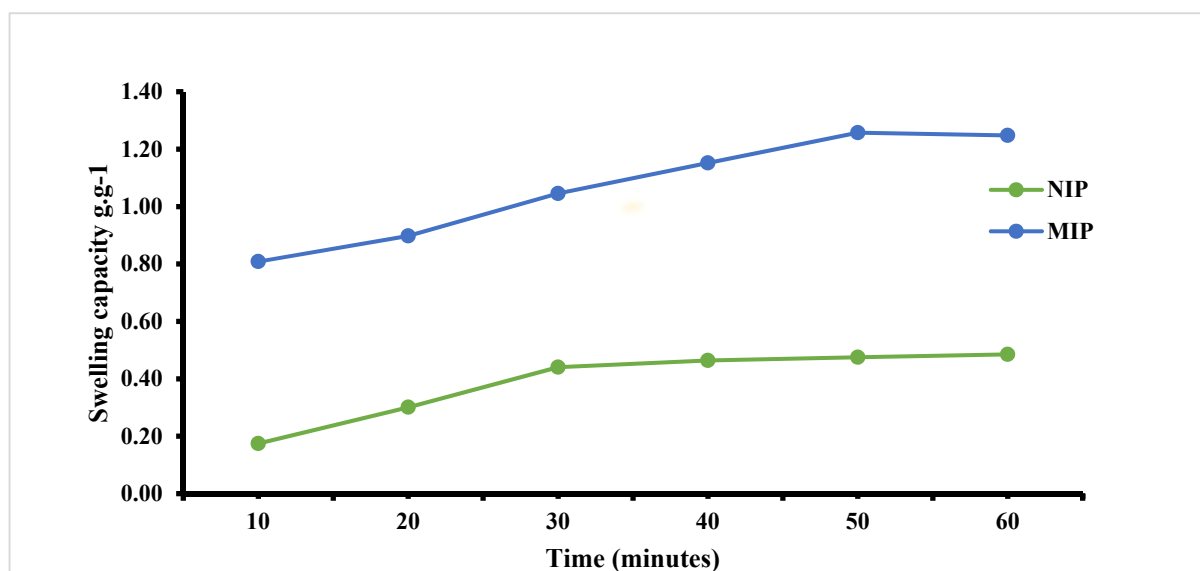


Figure 8. Swelling capacity of polymer as a function of time.

3.6. Selectivity Studies

The selectivity of the MIP was determined using Equations (7)–(9). Deionized water was spiked with 10 $\text{mg}\cdot\text{L}^{-1}$ of each target compound in the presence of equivalent quantities of acetaminophen, which was utilized as a competitor in a multi-component process. Acetaminophen is a popular analgesic drug with physicochemical properties and a size

similar to the target compounds [40]. It co-exists with all the mentioned target compounds in aquatic bodies. The competitor's molecular structure is similar to the target compounds in that they contain a carboxylic group. The hydrogen atom of the carboxylic group is predicted to interact with the nitrogen atom of 2-vinylpyridine, which is our functional monomer, as it should interact the same with acetaminophen. The MIP K' values were compared to acetaminophen to determine the effect of imprinting on selectivity. The compounds' binding capabilities on the MIP were found to be greater than those on the NIP. Table 5 summarizes the compound K_D , K , and K' values. EMI, TENO, NAP, DICLO, IBU, and EFV have K' values of 1.08, 1.0, 1.0, 1.0, 1.06, and 1.05, respectively, which are graphically represented in Figure 5. In aqueous samples, the selectivity of the MIP and NIP towards ARVs and NSAIDs in the presence of acetaminophen demonstrated that MIP has a slightly better selectivity towards the target compounds than the NIP.

Table 5. Template selectivity data in the presence of a competitor.

Templates	K_d MIP ($\text{mg}\cdot\text{g}^{-1}$)	K_d NIP ($\text{mg}\cdot\text{g}^{-1}$)	K (MIP)	K (NIP)	K'
Emtricitabine	1.78	1.65	1.16	1.06	1.08
Tenofovir disoproxil	1.78	1.77	1.44	1.44	1.00
Naproxen	1.77	1.76	1.14	1.14	1.00
Diclofenac	1.79	1.78	1.15	1.14	1.00
Ibuprofen	1.68	1.59	1.09	1.02	1.06
Efavirenz	1.81	1.74	1.17	1.12	1.05
Acetaminophen	1.56	1.55	-	-	-

The findings indicated that the MIP also shows significant adsorption efficiencies for five targeted compounds in the presence of the competitor. The order of the K_d values on the selectivity of MIP was EFV > TENO > DICLO > EMI > NAP, IBU than acetaminophen, which might imply that the imprinting cavities of the compounds were produced depending on the interplay of shape, size, quantity of hydrogen bonding, and functionality of the template. Some compounds are chosen over others, even in multi-template MIPs. The provided K_d values ranging from approximately 1.68 to 1.81 suggest a moderate affinity between the target molecule and the MIPs. These results are lower than those of Nkosi et al. [30], whose K_d values ranged between 1.0 and 3.9 for bulk polymerization of NSAIDs. These values indicate that the MIPs exhibit a consistent and reasonably strong binding capability toward the target molecule across multiple measurements. While not exceptionally high, these K_d values signify significant and reliable binding interactions, making the MIPs promising candidates for various applications requiring selective binding, such as chemical sensing, separation, and purification processes. Further optimization and characterization may be pursued to enhance the binding affinity and specificity of these MIPs for targeted applications.

3.7. Comparative Adsorbent Data

Table 6 presents a comparative assessment of adsorbents, including sol-gel materials, activated carbon, graphene oxide nanoplatelets, and others; bulk polymerization MIPs stand out as a promising alternative due to their unique molecular recognition capabilities. While sol-gel materials and certain adsorbents like activated carbon and graphene oxide nanoplatelets exhibit high adsorption capacities, they often suffer from limitations such as limited selectivity and susceptibility to fouling [41]. For instance, activated carbon, despite its high adsorption capacity, lacks molecular specificity and may be prone to fouling, reducing its efficiency over time. Similarly, graphene oxide nanoplatelets, while offering moderate to high adsorption capacities, pose concerns regarding availability and potential toxicity. In contrast, MIPs offer tailored molecular recognition, allowing for precise binding to specific target molecules. This specificity ensures efficient removal from complex

mixtures with minimal interference from other compounds. Moreover, MIPs demonstrate stability and can be regenerated and reused multiple times without significant loss of performance. Despite potential variations in adsorption capacities based on synthesis conditions, the advantages of molecular specificity and recyclability position MIPs as superior alternatives for applications requiring precise molecular recognition. Thus, MIPs offer a promising avenue for advancements in targeted adsorption tasks, overcoming the limitations posed by other materials.

Table 6. Comparison of the adsorption capacity and selectivity data found in pharmaceutical pollutants with other sorbents in the literature.

Adsorbent	Adsorption Capacity (mg/g)	Selectivity	Reference
Sol—gel	28.38	-	[42]
Raw zeolite	0.83	-	[43]
Activated carbon	90.9	-	[44]
Biosolid biochar	10.70	-	[45]
Graphene oxide nanoplatelet	38	-	[46]
MIP (NSAIDs)	1.230–1.249	1.12–2.4	[30]
MIP(ARV)	5.98	4.4	[32]
Chitosan MIP	79.41	-	[47]
Bulk polymerization (MIP)	0.92–3.92	1.68–1.81	This study

4. Conclusions

A multi-template MIP was successfully synthesized via a bulk polymerization process of ARVs and NSAIDs. The NMR and FTIR confirmed the successful cross-linking and removal of the templates, as there was not any difference in the chemical shifts and signal intensities. The TGA spectra revealed the two polymers have slight dissimilarities in their structures past 300 °C; however, both polymers had the backbone collapse beginning at 274 °C, suggesting they can withstand temperature up to that point. This was found satisfactory as the application of this material is at ambient temperatures. The SEM images revealed that the NIP has a smoother and more regular surface than the MIP; the MIP was more irregular and rougher due to the cavity removal and drying of the material. The target compound adsorption by the MIP was viable at pH 7.0. High extraction efficiencies and recoveries above 95% were observed for both the MIP and NIP in the adsorption of the target compounds. Adsorption kinetics were best fitted in the pseudo-second-order, which indicates that a chemisorption occurred. The selectivity of the MIP compared to the acetaminophen competitor was found to be slightly higher than the plain NIP.

Supplementary Materials: The following supporting information can be downloaded at: <https://www.mdpi.com/article/10.3390/app14083320/s1>, Figure S1: Mass effects of (a) MIP and (b) NIP for ARVs and NSAIDs recoveries; Figure S2: Effects of target initial concentration on the adsorption capacity with (a) MIP and (b) NIP; Figure S3: Extraction efficiency (a) MIP and (b) NIP based on template contact times.

Author Contributions: Conceptualization, S.S.; Methodology, S.S.; Formal analysis, S.S.; Investigation, S.S.; Writing—original draft, S.S.; Writing—review & editing, P.S.M.; Supervision, T.C.M., P.M.M., T.R.M. and T.H.M. All authors have read and agreed to the published version of the manuscript.

Funding: This research was funded by National Research Fund and Mitacs thematic program grant, grant number 122766.

Institutional Review Board Statement: Not applicable.

Informed Consent Statement: Not applicable.

Data Availability Statement: The data presented in this study are available on request from the corresponding author.

Acknowledgments: S.S. expresses gratitude to several grant sponsors and individuals who play pivotal roles in supporting and guiding research which is fundamental to the continuation of my research. She also wants to acknowledge and appreciate S’busiso Nkosi for their unwavering support, mentorship, and invaluable knowledge-sharing.

Conflicts of Interest: The authors declare no conflict of interest.

References

1. Patel, M.; Kumar, R.; Kishor, K.; Mlsna, T.; Pittman, C.U.; Mohan, D. Pharmaceuticals of emerging concern in aquatic systems: Chemistry, occurrence, effects, and removal methods. *Chem. Rev.* **2019**, *119*, 3510–3673. [[CrossRef](#)] [[PubMed](#)]
2. Ebele, A.J.; Oluseyi, T.; Drage, D.S.; Harrad, S.; Abdallah, M.A.-E. Occurrence, seasonal variation and human exposure to pharmaceuticals and personal care products in surface water, groundwater and drinking water in Lagos State, Nigeria. *Emerg. Contam.* **2020**, *6*, 124–132. [[CrossRef](#)]
3. Lin, J.Y.; Zhang, Y.; Bian, Y.; Zhang, Y.X.; Du, R.Z.; Li, M.; Tan, Y.; Feng, X.-S. Non-steroidal anti-inflammatory drugs (NSAIDs) in the environment: Recent updates on the occurrence, fate, hazards and removal technologies. *Sci. Total Environ.* **2023**, *904*, 166897. [[CrossRef](#)] [[PubMed](#)]
4. Ahammad, N.A.; Ahmad, M.A.; Hameed, B.H.; Din, A.T.M. A mini review of recent progress in the removal of emerging contaminants from pharmaceutical waste using various adsorbents. *Environ. Sci. Pollut. Res.* **2023**, *30*, 124459–124473. [[CrossRef](#)] [[PubMed](#)]
5. Couto, C.F.; Lange, L.C.; Amaral, M.C.S. Occurrence, fate and removal of pharmaceutically active compounds (PhACs) in water and wastewater treatment plants—A review. *J. Water Process Eng.* **2019**, *32*, 100927. [[CrossRef](#)]
6. K’oreje, K.O.; Vergeynst, L.; Ombaka, D.; De Wispelaere, P.; Okoth, M.; Van Langenhove, H.; Demeestere, K. Occurrence patterns of pharmaceutical residues in wastewater, surface water and groundwater of Nairobi and Kisumu city, Kenya. *Chemosphere* **2016**, *149*, 238–244. [[CrossRef](#)] [[PubMed](#)]
7. K’oreje, K.O.; Okoth, M.; Van Langenhove, H.; Demeestere, K. Occurrence and treatment of contaminants of emerging concern in the African aquatic environment: Literature review and a look ahead. *J. Environ. Manag.* **2020**, *254*, 109752. [[CrossRef](#)]
8. Osman, A.I.; Ayati, A.; Farghali, M.; Krivoschapkin, P.; Tanhaei, B.; Karimi-Maleh, H.; Krivoschapkina, E.; Taheri, P.; Tracey, C.; Al-Fatesh, A.; et al. *Advanced Adsorbents for Ibuprofen Removal from Aquatic Environments: A Review*; Springer International Publishing: Berlin/Heidelberg, Germany, 2023; Volume 22, no. 1. [[CrossRef](#)]
9. Abafe, O.A.; Späth, J.; Fick, J.; Jansson, S.; Buckley, C.; Stark, A.; Pietruschka, B.; Martincigh, B.S. LC-MS/MS determination of antiretroviral drugs in influents and effluents from wastewater treatment plants in KwaZulu-Natal, South Africa. *Chemosphere* **2018**, *200*, 660–670. [[CrossRef](#)]
10. Ncube, S.; Madikizela, L.M.; Chimuka, L.; Nindi, M.M. Environmental fate and ecotoxicological effects of antiretrovirals: A current global status and future perspectives. *Water Res.* **2018**, *145*, 231–247. [[CrossRef](#)]
11. Kasonga, T.K.; Coetzee, M.A.A.; Kamika, I.; Ngole-Jeme, V.M.; Momba, M.N.B. Endocrine-disruptive chemicals as contaminants of emerging concern in wastewater and surface water: A review. *J. Environ. Manag.* **2021**, *277*, 111485. [[CrossRef](#)]
12. Archer, E.; Petrie, B.; Kasprzyk-Hordern, B.; Wolfaardt, G.M. The fate of pharmaceuticals and personal care products (PPCPs), endocrine disrupting contaminants (EDCs), metabolites and illicit drugs in a WWTW and environmental waters. *Chemosphere* **2017**, *174*, 437–446. [[CrossRef](#)] [[PubMed](#)]
13. Sigonya, S.; Mokhothu, T.H.; Mokhena, T.C.; Makhanya, T.R. Mitigation of Non-Steroidal Anti-Inflammatory and Antiretroviral Drugs as Environmental Pollutants by Adsorption Using Nanomaterials as Viable Solution—A Critical Review. *Appl. Sci.* **2023**, *13*, 772. [[CrossRef](#)]
14. Raupp, Í.N.; Filho, A.V.; Arim, A.L.; Muniz, A.R.C.; da Rosa, G.S. Ibuprofen Adsorption onto Olive Pomace Activated Carbon. *Chem. Eng. Technol.* **2023**, *46*, 2395–2403. [[CrossRef](#)]
15. Escobar, J.; Hernández, L.; González, J.L.; Salazar-González, R.; Calzadilla, W.; Guerrero, L.; Escalona, N.; Huilñir, C. Removal of Ibuprofen and Diclofenac in Batch Nitrifying Reactors: Effect of Natural Zeolite on the Process. *Water* **2023**, *15*, 2665. [[CrossRef](#)]
16. Bukhari, A.A.H. Preparation of molecularly imprinted silica particles with amino functionality for chiral separation of (±)-naproxen. *Chirality* **2023**, *35*, 311–322. [[CrossRef](#)] [[PubMed](#)]
17. Bouzidi, M.; Sellaoui, L.; Mohamed, M.; Franco, D.S.P.; Erto, A.; Badawi, M. A comprehensive study on paracetamol and ibuprofen adsorption onto biomass-derived activated carbon through experimental and theoretical assessments. *J. Mol. Liq.* **2023**, *376*, 121457. [[CrossRef](#)]
18. Popaliya, M.; Mishra, A. Modified zeolite as an adsorbent for dyes, drugs, and heavy metal removal: A review. *Int. J. Environ. Sci. Technol.* **2023**, *20*, 12919–12936. [[CrossRef](#)]
19. Li, M.; Xiao, J.; Chen, L.; Ren, B.; Liu, Z.; Guo, Y.; Wang, Y. A study of the optimal diffusion distance of ibuprofen through the synthesis of different sizes of mesoporous silica. *J. Solid State Chem.* **2023**, *321*, 123911. [[CrossRef](#)]
20. Gkika, D.A.; Tolkou, A.K.; Lambropoulou, D.; Bikiaris, D.N.; Kokkinos, P.; Kalavrouziotis, I.K.; Kyzas, G.Z. Application of molecularly imprinted polymers (MIPs) as environmental separation tools. *RSC Appl. Polym.* **2024**, *2*, 127–148. [[CrossRef](#)]

21. Pilvenyte, G.; Ratautaite, V.; Boguzaitė, R.; Ramanavicius, A.; Viter, R.; Ramanavicius, S. Molecularly Imprinted Polymers for the Determination of Cancer Biomarkers. *Int. J. Mol. Sci.* **2023**, *24*, 4105. [[CrossRef](#)]
22. Rodríguez-Saldaña, V.; Castro-García, C.; Rodríguez-Maese, R.; Leal-Quezada, L.O. Advances in the extraction methods for the environmental analysis of non-steroidal anti-inflammatory drugs (NSAIDs). *TrAC-Trends Anal. Chem.* **2023**, *169*, 117409. [[CrossRef](#)]
23. Gupta, Y.; Beckett, L.E.; Sadula, S.; Vargheese, V.; Korley, L.S.T.J.; Vlachos, D.G. Bio-based molecular imprinted polymers for separation and purification of chlorogenic acid extracted from food waste. *Sep. Purif. Technol.* **2023**, *327*, 124857. [[CrossRef](#)]
24. Zhang, X.; Shen, F.; Zhang, Z.; Xing, Y.; Ren, X. Synthesis of a novel cross-linker doubles as a functional monomer for preparing a water compatible molecularly imprinted polymer. *Anal. Methods* **2014**, *6*, 9483–9489. [[CrossRef](#)]
25. Zunngu, S.S.; Madikizela, L.M.; Chimuka, L.; Mdluli, P.S. Synthesis and application of a molecularly imprinted polymer in the solid-phase extraction of ketoprofen from wastewater. *Comptes Rendus Chim.* **2017**, *20*, 585–591. [[CrossRef](#)]
26. Mehmandoust, M.; Soylak, M.; Erk, N. Innovative molecularly imprinted electrochemical sensor for the nanomolar detection of Tenofovir as an anti-HIV drug. *Talanta* **2023**, *253*, 123991. [[CrossRef](#)] [[PubMed](#)]
27. Hasanah, A.N.; Susanti, I. Molecularly Imprinted Polymers for Pharmaceutical Impurities: Design and Synthesis Methods. *Polymers* **2023**, *15*, 3401. [[CrossRef](#)] [[PubMed](#)]
28. Bognár, Z.; Kozma, J.; Kovács, N.; Gyurcsányi, R.E. Novel functional monomer for the electrochemical synthesis of highly affine epitope-imprinted polymers. *Electroanalysis* **2023**, *35*, e202300025. [[CrossRef](#)]
29. Sigonya, S.; Chibuzor, S.; Phumlani, O.; Mdluli, S.; Hendrica, T. Method optimisation and application based on solid phase extraction of non steroidal anti-inflammatory drugs, antiretroviral drugs, and a lipid regulator from coastal areas of Durban, South Africa. *SN Appl. Sci.* **2022**, *4*, 231. [[CrossRef](#)]
30. Nkosi, S.M.; Mahlambi, P.N.; Chimuka, L. Synthesis, characterisation and optimisation of bulk molecularly imprinted polymers from nonsteroidal anti-inflammatory drugs. *S. Afr. J. Chem.* **2022**, *76*, 56–64. [[CrossRef](#)]
31. Madikizela, L.M.; Chimuka, L. Determination of ibuprofen, naproxen and diclofenac in aqueous samples using a multi-template molecularly imprinted polymer as selective adsorbent for solid-phase extraction. *J. Pharm. Biomed. Anal.* **2016**, *128*, 210–215. [[CrossRef](#)]
32. Qwane, S.N.; Mdluli, P.S.; Madikizela, L.M. Synthesis, Characterization and Application of a Molecularly Imprinted Polymer in Selective Adsorption of Abacavir from Polluted Water. *S. Afr. J. Chem.* **2020**, *73*, 84–91. [[CrossRef](#)]
33. Madikizela, L.M.; Chimuka, L. Synthesis, adsorption and selectivity studies of a polymer imprinted with naproxen, ibuprofen and diclofenac. *J. Environ. Chem. Eng.* **2016**, *4*, 4029–4037. [[CrossRef](#)]
34. Mbhele, Z.E.; Ncube, S.; Madikizela, L.M. Synthesis of a molecularly imprinted polymer and its application in selective extraction of fenoprofen from wastewater. *Environ. Sci. Pollut. Res.* **2018**, *25*, 36724–36735. [[CrossRef](#)] [[PubMed](#)]
35. Orimi, S.M.H.; Khavarpour, M.; Kazemi, S. Removal of bisphenol A from water solution using molecularly imprinted nanoparticles: Isotherm and kinetic studies. *J. Water Environ. Nanotechnol.* **2020**, *5*, 56–67. [[CrossRef](#)]
36. Liu, X.; Tian, L.; Ren, R.; Wang, T.; Wang, Y. Constructing hollow ZIF-8/CDs@MIPs fluorescent sensor from Osmanthus leaves to specifically recognize bovine hemoglobin. *Spectrochim. Acta—Part A Mol. Biomol. Spectrosc.* **2023**, *287*, 122121. [[CrossRef](#)] [[PubMed](#)]
37. Zidarič, T.; Majer, D.; Maver, T.; Finšgar, M.; Maver, U. The development of an electropolymerized, molecularly imprinted polymer (MIP) sensor for insulin determination using single-drop analysis. *Analyst* **2023**, *148*, 1102–1115. [[CrossRef](#)]
38. Sikiti, P.; Msagati, T.A.M.; Mamba, B.B.; Mishra, A.K. Synthesis and characterization of molecularly imprinted polymers for the remediation of PCBs and dioxins in aqueous environments. *J. Environ. Health Sci. Eng.* **2014**, *12*, 82. [[CrossRef](#)] [[PubMed](#)]
39. Madikizela, L.M.; Mdluli, P.S.; Chimuka, L. Experimental and theoretical study of molecular interactions between 2-vinyl pyridine and acidic pharmaceuticals used as multi-template molecules in molecularly imprinted polymer. *React. Funct. Polym.* **2016**, *103*, 33–43. [[CrossRef](#)]
40. Kaya, Y.; Ersan, G.; Vergili, I.; Gönder, Z.B.; Yilmaz, G.; Dizge, N.; Aydiner, C. The treatment of pharmaceutical wastewater using in a submerged membrane bioreactor under different sludge retention times. *J. Memb. Sci.* **2013**, *442*, 72–82. [[CrossRef](#)]
41. Ali, I.; Zenab, S.; Garcia, H.; Danquah, M.K.; Imanova, G. Recent advances in graphene-based nano-membranes for desalination. *Chem. Eng. J.* **2024**, *483*, 149108. [[CrossRef](#)]
42. Liu, D.; Zhao, K.; Qi, M.; Li, S.; Xu, G.; Wei, J.; He, X. Preparation of protein molecular-imprinted polysiloxane membrane using calcium alginate film as matrix and its application for cell culture. *Polymers* **2018**, *10*, 170. [[CrossRef](#)] [[PubMed](#)]
43. Negarestani, M.; Mollahosseini, A.; Farimaniraad, H.; Ghiasinejad, H.; Shayesteh, H.; Kheradmand, A. Efficient removal of non-steroidal anti-inflammatory ibuprofen by polypyrrole-functionalized magnetic zeolite from aqueous solution: Kinetic, equilibrium, and thermodynamic studies. *Sep. Sci. Technol.* **2023**, *58*, 435–453. [[CrossRef](#)]
44. Farghal, H.H.; Nebsen, M.; El-Sayed, M.M.H. Eco-friendly Biopolymer/Activated Charcoal Magnetic Nanocomposites with Enhanced Stability and Adsorption Properties for Water Treatment Applications. *J. Polym. Environ.* **2023**, *31*, 5338–5354. [[CrossRef](#)]
45. Oh, S.Y.; Seo, Y.D. Sorption of halogenated phenols and pharmaceuticals to biochar: Affecting factors and mechanisms. *Environ. Sci. Pollut. Res.* **2016**, *23*, 951–961. [[CrossRef](#)] [[PubMed](#)]

46. Hummadi, K.K.; Luo, S.; He, S. Adsorption of methylene blue dye from the aqueous solution via bio-adsorption in the inverse fluidized-bed adsorption column using the torrefied rice husk. *Chemosphere* **2022**, *287*, 131907. [[CrossRef](#)]
47. Stachowiak, M.; Cegłowski, M.; Kurczewska, J. Hybrid chitosan/ molecularly imprinted polymer hydrogel beads doped with iron for selective ibuprofen adsorption. *Int. J. Biol. Macromol.* **2023**, *251*, 126356. [[CrossRef](#)]

Disclaimer/Publisher's Note: The statements, opinions and data contained in all publications are solely those of the individual author(s) and contributor(s) and not of MDPI and/or the editor(s). MDPI and/or the editor(s) disclaim responsibility for any injury to people or property resulting from any ideas, methods, instructions or products referred to in the content.